



Article

Performance Enhancement of a Multiresonant Piezoelectric Energy Harvester for Low Frequency Vibrations

Iman Izadgoshasb ^{*}, Yee Yan Lim, Ricardo Vasquez Padilla, Mohammadreza Sedighi  and Jeremy Paul Novak

School of Environment, Science and Engineering, Southern Cross University, East Lismore, NSW 2480, Australia

* Correspondence: iman.izadgoshasb@scu.edu.au

Received: 28 June 2019; Accepted: 17 July 2019; Published: 19 July 2019



Abstract: Harvesting electricity from low frequency vibration sources such as human motions using piezoelectric energy harvesters (PEH) is attracting the attention of many researchers in recent years. The energy harvested can potentially power portable electronic devices as well as some medical devices without the need of an external power source. For this purpose, the piezoelectric patch is often mechanically attached to a cantilever beam, such that the resonance frequency is predominantly governed by the cantilever beam. To increase the power generated from vibration sources with varying frequency, a multiresonant PEH (MRPEH) is often used. In this study, an attempt is made to enhance the performance of MRPEH with the use of a cantilever beam of optimised shape, i.e., a cantilever beam with two triangular branches. The performance is further enhanced through optimising the design of the proposed MRPEH to suit the frequency range of the targeted vibration source. A series of parametric studies were first carried out using finite-element analysis to provide in-depth understanding of the effect of each design parameters on the power output at a low frequency vibration. Selected outcomes were then experimentally verified. An optimised design was finally proposed. The results demonstrate that, with the use of a properly designed MRPEH, broadband energy harvesting is achievable and the efficiency of the PEH system can be significantly increased.

Keywords: piezoelectric energy harvesting; renewable energy; low frequency; multiresonant

1. Introduction

Using renewable macroenergy harvesting systems like solar energy [1–6] or wind energy [7–10] has become popular over the past few decades. In recent years, the advancement of new methods and applications of wireless networks drives the demand on microenergy harvesting for continuous power supply [11]. Among these various renewable energy sources, such as biomass [12,13], heat [14] and vibration [15,16], vibration-based energy harvesting has attracted the interest of many researchers because of the ubiquity and availability of various vibration sources. In addition to energy harvesting, piezoelectric materials have a wide range of applications [17–21] in various science and engineering disciplines.

Vibrational energy harvesters can be divided into several categories based on their energy conversion mechanisms, such as electrostatic, electrodynamic and piezoelectric energy harvesters [22]. Generally, electrodynamic conversion methods are used to harvest energy from high-frequency vibration sources while piezoelectric materials are more suitable for converting mechanical energy to electrical energy for low-frequency excitations. Several other factors can also affect the choice of harvesters, including size, weight, stability and total cost of the device to be powered.

Piezoelectric energy harvesters (PEH) are easy to fabricate at relatively low cost, rendering it highly attractive. Although many studies have been conducted to increase the efficiency of the PEH, including broadband piezoelectric vibration energy harvesting [22,23], the desired efficiency is yet to be achieved. The ultimate output power of PEHs is influenced by a range of factors including the material properties, the geometry and properties of the substrate at which the PEH is attached [24,25], the weight and position of proof mass [26,27], the performance of AC/DC circuit [28,29], the coupling coefficient, as well as the parasitic damping [30].

In application, the PEH is often mechanically attached to a metallic cantilever beam, such that the resonance frequency is predominantly governed by the cantilever beam. It is common to use only the fundamental vibration mode of this PEH cantilever beam (PEHCB) system. The higher modes are usually separated from the fundamental mode and are considered less useful for broadband energy harvesting. This, in turn, results in one of the major drawbacks of the PEH—its poor performance when the excitation frequency of the vibrating source is away from the resonance frequency. Thus, it is essential for researchers to create new designs capable of performing at broader frequency range, i.e., broadband energy harvesting. One of the possible designs is the use of multimodal PEH, which possesses multiple resonance frequencies within a desirable range.

To achieve multiple resonance peaks, researchers have attempted to change the configuration of the PEHCB through relocating the mass, changing the geometry of the cantilever beam, using several PEHCB in parallel, varying the thickness of the PEHCB [16,31,32] or using magnets [33]. Xue et al. [34] studied the integration of multiple bimorphs with various thicknesses for broadband energy scavenging. Ferrari et al. [35] later suggested the use of several PEHCB with different resonance frequencies in parallel. Erturk et al. [36] proposed an L-shaped piezoelectric structure with the first two resonance frequencies at 16.4 and 49.3 Hz, respectively. Their device was designed to be used in the landing gear of unmanned air vehicles.

Later in 2011, Kim et al. [37] designed a 2-DOF PEH in which two cantilever beams are connected through a rigid mass. Rotational and translational motions of the mass are used for tuning the resonance frequencies such that they are close to each other. Further investigations by Wu et al. [38] have shown that a 2-DOF PEH system (comprising of inner and outer cantilevers) is able to increase the output power. In their proposed design, the proof masses attached to both beams were adjustable for wider bandwidth. Zhang and Hu [39] proposed a PEH system which includes a few branches of cantilever beams with proof masses at their free ends. They were connected to the main cantilever beam with PEH attached. This setup was able to generate multiple resonance peaks at different frequencies.

Studies have also been conducted on the incorporation of magnetic interactions into the PEH system for inducing nonlinear stiffness, to widen the bandwidth of the PEH. For instance, Challa et al. [33] used the magnetic interactions to alter the stiffness of the PEHCB for passive tuning of resonance frequency. In spite of the fact that magnetic forces can provide bidirectional resonance tuning [40], traversing the magnets in practice is very difficult and the power required for execution is nearly equal to the harvested power [41]. In another study, Tang and Yang [42] proposed a nonlinear PEH design incorporating a magnetic oscillator for improving the operational bandwidth and for increasing the output power. A 100% increase in the operational bandwidth and nearly 40% improvement of the harvested power under 0.2g excitation was achieved.

Although many attempts have been made to achieve multiple resonances [43], an effective technique remains highly sought after. Sordo et al. [44] introduced a PEH system containing several cantilever beams with various geometries that were attached to another cantilever beam with piezoelectric patch. As each beam can produce resonance at a specific frequency, the system possesses several resonance frequencies which could better match the excitation frequency of the vibration source.

Wu et al. [45] investigated the wideband PEH consisting of three masses and an asymmetric M-shaped cantilever beam. The M-shape beam comprises a main beam and two folded and dimension varied auxiliary beams interconnected through the proof mass at the end of the main cantilever beam. Their device was able to produce multiple resonance frequencies ranging from 14.3 to 23.4 Hz. Their

work was followed by Upadrashta et al. [46,47] where three rectangular cantilever beams with various sizes were attached to the main cantilever beam using bolts. They conducted finite element analysis (FEA) to search for the best geometry of each beam. As a result, the PEH system can generate several resonance frequencies between 15 and 20 Hz.

To apply this method, the base of the cantilever beam should have sufficient space to fit several branches of cantilever beams and perhaps requires a larger piezoelectric patch and higher base acceleration to generate enough power. In addition, the efficiency of harvester may decline as the branched cantilever beams are attached to the main beam through bolts or bonding, rendering the harvester nonhomogenous. On the other hand, to harvest energy from a low frequency environment, say below 10 Hz, the harvester needs to be downscaled, leading to difficulty in the fabrication process. As such, changing the geometry of the main piezoelectric cantilever beam instead of attaching several branched beams can be a solution.

In this paper, an attempt is made to design an efficient multimodal PEH system with two close resonance frequencies. This proposed harvester, termed multiresonant PEH (MRPEH) [48], consists of one piezoelectric patch attached to a cantilever beam with two triangular branches. This proposed harvester was further optimised in this research by varying a range of design parameters, so as to achieve high energy output with minimum volume and weight of material. This is especially useful for applications where weight and size are serious penalties. This design is expected to generate high power across wide frequency bandwidth for low frequency random vibration sources such as human motions [49].

This paper is structured as follows: Section 2 presents the design of the proposed MRPEH and presents numerical studies on the design through finite-element modelling. In Section 3, a parametric study is carried out to optimise the design of the MRPEH to achieve close resonances at low frequency spectrum. The experimental setup is then presented and the performance of the proposed MRPEH under harmonic excitation is experimentally studied as narrated in Section 4. Conclusion is presented in Section 5.

2. Design of Multiresonant Piezoelectric Energy Harvester

The proposed MRPEH comprises of a main aluminium cantilever beam (30 mm × 20 mm) with a piezoelectric patch–macrofibre composite (MFC M2814-P2) attached near the clamped end and two branches of smaller triangular beams with tip masses (M1 and M2), as schematically presented in Figure 1. The length of the branched cantilevers are denoted as L1 and L2.

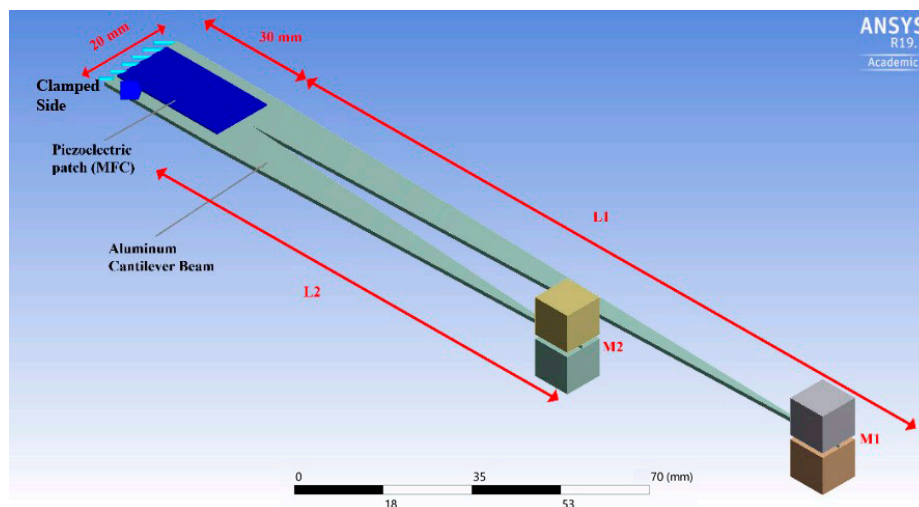


Figure 1. Schematic of the proposed multiresonant piezoelectric energy harvester (MRPEH) design.

Under base excitation, the vertical displacements of both branched beams are transferred to the main beam, resulting in bending of the piezoelectric patch, thus generating power. As each branched beam has different fundamental resonance frequencies, closely spaced resonance frequencies can be tuned. Cantilever beams of triangular shape were chosen based on a previous study [50]. Further analysis was performed using FEA to optimize the geometry of the cantilever beam. The parameters under consideration include the material properties of the cantilever beam, its geometry and the weight of the proof masses. These parameters affect the vibratory response of the MRPEH, in particular, the resonance frequencies. The optimum lengths for branched triangular beams (L1 and L2) are evaluated through a parametric study using ANSYS as presented in the next section. The impact of proof masses of different weight on the harvested power is also investigated. The targeted frequency range for this research study lies between 1 Hz and 20 Hz, with particular interest given to frequencies below 10 Hz. The objective is to optimise the geometry in order to produce two close resonance frequency within the frequency range of interest. In other words, the proposed MRPEH can be tuned to produce multiple resonances based on the frequency range of the targeted vibration source. The fabricated prototype of the proposed MRPEH was then experimentally tested under harmonic base excitation as presented in Section 4.

3. Finite Element Analysis of MRPEH

Finite element analysis software is a powerful tool to solve complex engineering problems [51]. Commercial FEA software packages such as ANSYS possess advanced capability of solving coupled field problems involving complex piezoelectric interactions.

In 2009, Elvin and Elvin [52] introduced the coupled field finite element method (FEM) and circuit simulation approach for analysing the performance of PEH. They proposed that the mechanical behaviour of the PEHCB can be simulated using FEM packages like ANSYS while circuit analysis can be performed using standard circuit simulation software such as SPICE. Later, Yang and Tang [53] introduced an equivalent circuit model to evaluate the performance of complex mechanical systems with the circuit having nonlinear electrical components. ANSYS and SPICE software were again used for simulation. In another study, Arafa et al. [54] evaluated the performance of a PEHCB with a dynamic magnifier using FEM. The proposed dynamic magnifier contained a spring mass system which was placed between the fixed end of PEHCB and the vibration source. The dynamic magnifier was able to magnify the strain in the piezoelectric patch and thus amplify the power output. Subsequently, Thein and Liu [55] made an attempt to analyse the performance of PEH systems using FEA. A parametric study was conducted in the FEA using ANSYS to find the best geometry of the cantilever beam.

Recently, ANSYS introduced “Piezo & MEMS ACT extension” which is an add-on to the ANSYS workbench. In this research “ANSYS Workbench R19.1 Academic” with “Piezo & MEMS ACT extension” is employed for static structural, modal, and harmonic analysis. The main and branched cantilever beam, as well as the tip masses, were modelled with 3D, hexahedral elements (SOLID186) which have 20 nodes and three translational DOFs at each node in three directions (x -, y -, z -). The piezoelectric material was modelled with a 3D, 20-node SOLID226 piezoelectric element. This element has an additional electric potential DOF at each node in addition to the three translational DOFs. Bending, compression and shear modes of the beam can be modelled accordingly.

In this study, the bending mode (d_{31}) of the MFC patch attached on the MRPEH was excited by a controlled base excitation. The material properties of the MFC are tabulated in Table 1. The resistance was set to 1 M Ω to emulate open circuit condition. It is worth mentioning that an open circuit is mathematically treated as infinite resistance. In FEM analysis, it is common [46] to use a very large resistance, such as 1 M Ω to emulate a practically “infinite” resistance.

Table 1. Material properties of multiresonant PEH.

Parameter	Substrate (Cantilever Beam)	Piezoelectric
Material	Aluminium 7075-T6	MFC M2814-P2
Elastic modulus (GPa)	69.5	30.336
Poisson's ratio	0.33	0.31
Density (kg/m ³)	2700	5400
Piezoelectric constant (c/m ²)	-	-5.16
Capacitance (nF)	-	30.8

One end of the beams was fixed to simulate the clamped boundary condition. The size of the element used to simulate the MRPEH should be sufficiently fine to obtain accurate results but not excessively small to avoid unduly long computational time. The size of the element was chosen as 0.8 mm which is small enough to produce accurate results according to [55]. Acceleration at the fixed end of the cantilever beam was controlled at 0.2g [46].

To obtain the highest efficiency, the geometry should not only be optimised to produce several resonances within the frequency range of the targeted vibration source, but also should have the ability to generate reasonably high voltage. Thus, creating a few high voltage resonances close to each other is desirable for such PEH. As higher strain is the key to generating a higher voltage, the geometry of the branched beams of the proposed MRPEH (Figure 1) should be designed to experience the highest strain. According to the literature [55], a triangular cantilever beam produces higher strain than a rectangular counterpart. Therefore, in this study, the design of the branched beams of the MRPEH is chosen to be triangular in shape.

The following section presents the results of static structural analysis obtained from FEA. The stress, strain and deflection of rectangular and triangular beams were compared.

Next, modal analysis was carried out to find the first six resonances of the MRPEH within the target frequency range. The length of the cantilever beam and the weight of tip masses were carefully selected by conducting a parametric study. Finally, the dynamic response of the MRPEH under base excitation was evaluated through harmonic analysis.

3.1. Static Structural Analysis of Cantilever Beam

Numerous studies have been conducted to find the best geometry of PEHCB. The triangular shape was selected by several researchers [24,55] because of its ability to yield high strain and stress across the beam's length when loaded. The piezoelectric patch is able to produce high power when the strain across the beam is high.

In this section, the performance of the triangular shape branched beam is studied using static structural analysis and is compared with the rectangular beam. With one side of both beams fixed, a 0.5 N point load is applied at the free end of each beam. The length of both beams is 190 mm and the width of the fixed end is 20 mm. The beams were assumed to be made of aluminium (Grade T6061). The material properties used for this simulation are summarized in Table 1.

Table 2 tabulates the estimated deformation, strain and stress of both beams. The maximum stress on the rectangular beam is 30 MPa and the minimum is about 3.8 kPa. These values decrease over the length of rectangular beam. The minimum stress of the triangular beam is 7.1 kPa which is much higher than the similar magnitude of the rectangular beam. The maximum stress is 31 MPa which is close to the rectangular beam but it does not decrease linearly and remains predominantly constant throughout the length of the triangular beam. For ease of comparison, the average stress is considered. In this case, the average stresses for rectangular beam and triangular beam are 12 MPa and 24 MPa, respectively. The average stress of the triangular geometry is twice that of the rectangular counterpart.

Table 2. Magnitudes of stress and strain with rectangular and triangular beams.

Beam Shape		Min	Max	Average
Rectangular Beam	Deformation (m)	0	9.51×10^{-3}	3.56×10^{-3}
	Strain (m/m)	6.33×10^{-7}	4.32×10^{-4}	1.98×10^{-4}
	Stress (MPa)	$0.38 \times 10^{+1}$	$3.06 \times 10^{+3}$	1.20×10^{-3}
Triangular Beam	Deformation (m)	0	1.44×10^{-2}	2.92×10^{-3}
	Strain (m/m)	1.38×10^{-4}	4.41×10^{-4}	3.96×10^{-4}
	Stress (MPa)	$0.72 \times 10^{+1}$	$3.13 \times 10^{+3}$	$2.39 \times 10^{+3}$

A similar trend can be observed from the strain distribution where the average strain of the rectangular beam is 1.98×10^{-4} and is 3.96×10^{-4} for the triangular beam. These analyses justify the use of the triangular shape beam as the amount of strain is greatly increased under similar loading condition, which is expected to increase the power output of the piezoelectric patch. Therefore, the following study adopts triangular branched beams in the MRPEH. It is noticeable that triangular beams have lower volume compared to rectangular beams, which is very important in some applications, such as human motion energy harvesters.

3.2. Parametric Study of Cantilever Beam with Tip Mass


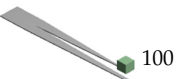
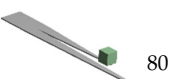
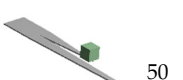


Resonance frequencies and modal characteristics of the MRPEH are expected to change when the parameters of the cantilever beam, such as length, width, thickness or tip mass, are changed. A parametric study was first conducted to understand the effect of each parameter and to search for an optimum design for the cantilever beam with tip mass in the low frequency spectrum (1–10 Hz). The objective is to produce two closely spaced fundamental resonance frequencies below 10 Hz. One way of conducting such a parametric study is by solving the analytical equations for multi-DOF systems. However, despite the existence of closed-form solutions for simple structures such as cantilever beams, solutions of models with complex geometries and boundary conditions are often unavailable. A few studies have been conducted using lumped parameter models to analyse 1-DOF or 2-DOF piezoelectric systems [56–58] but the accuracy of the solution was compromised. To overcome the above-mentioned shortcoming, the FE model was selected in this study. In Section 3.2, modal analysis was conducted in ANSYS workbench to determine the natural frequencies and the mode shapes of the cantilever beam.

In the parametric study, the lengths (L1 and L2) of both branched beams (as shown in Figure 1) were varied and modal analyses were performed to seek two appropriately spaced resonance frequencies. Since the commercially available piezoelectric patch is 30 mm in length, the minimum length of the branched beams was taken as 50 mm to be functional. On the other hand, the maximum length of the branched beam was limited to 160 mm to avoid bending and early fatigue failure. To analyse the impact of varying length (Section 3.2.1), the thickness of the beam and the weight of the tip masses were first kept at 1 mm and 40 g (each), respectively. A separate analysis was then carried out (Section 3.2.2) to study the effect of varying tip masses. Note that at this stage, only the behaviour of the cantilever beam is considered.

3.2.1. Effect of Length of Branched Beams

Table 3 illustrates the six schematics of cantilever beams with varying lengths of L1 and L2. With the modal analysis conducted, the first six natural frequencies of each design are summarized in the table. Selecting the best geometry for the design of MRPEH strongly depends on the frequency spectrum of the target vibration source. In this research, the frequency of target vibration source was considered to be lower than 20 Hz, with frequencies below 10 Hz being of main interest.

Table 3. Various geometries of branched beams and their natural frequencies (NF: natural frequency).

Design No.	Geometry	L1 (mm)	L2 (mm)	NF1 (Hz)	NF2 (Hz)	NF3 (Hz)	NF4 (Hz)	NF5 (Hz)	NF6 (Hz)
1		160	160	3.343	3.945	17.197	17.312	51.828	55.506
2		100	160	3.592	6.630	17.135	32.782	51.404	62.994
3		80	160	3.616	9.86	17.123	49.037	51.406	62.928
4		50	160	3.616	16.579	17.142	51.623	62.88	79.534
5		50	100	6.348	16.94	32.304	76.176	78.667	101.14
6		80	80	8.234	11.46	46.563	48.014	87.346	98.928

For Design no. 1 to 4, the first three resonance frequencies fall below 20 Hz and for Design no. 1 to 3, the first two resonant frequencies are less than 10 Hz. Therefore, Design no. 5 and 6 were not suitable for this study. For Design no. 1 to 4, the first three resonance frequencies were less than 20 Hz, but since the vibration source is expected to operate mainly below 10 Hz, Design no. 4 was less preferable. For Design no. 1, two excessively close resonance frequencies were observed, which is not suitable for this application. Both Design no. 2 and 3 perform well below 10 Hz. It is worth mentioning again that optimisation of the geometry is mainly governed by the target frequency range. In this study, Design no. 2 in Table 3 was eventually chosen for further analysis because of its two closely spaced resonance frequencies below 10 Hz (3.5 Hz and 6.6 Hz). Design no. 2 was also fabricated for the upcoming experimental study.

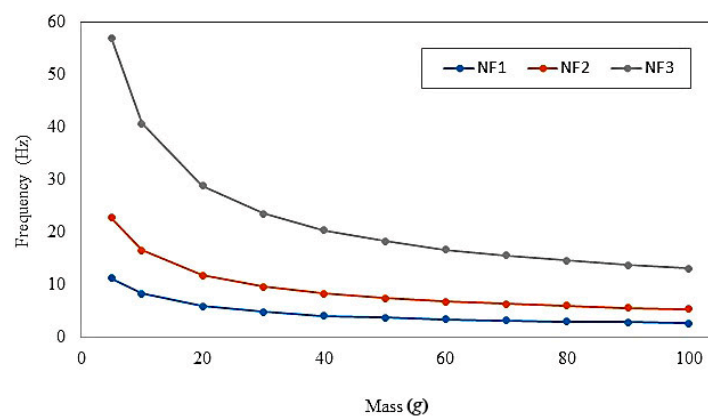
3.2.2. Effect of Varying Tip Mass

The weight of tip masses at the free end of the branched beams are also expected to affect the resonance frequencies of the MRPEH. To understand the effect, a range of masses, from 5 g to 100 g, was applied at the tip of the branched beams. Modal analyses were then repeatedly conducted. Table 4 shows the first three resonant frequencies of the selected cantilever beam (Design no. 2) with different tip masses.

Although the increase in tip mass can effectively reduce the resonance frequency, the effect is less pronounced when the mass exceeds 40 g, as shown in Figure 2. This is particularly obvious in the case of the first and second natural frequencies. Selecting the weight of tip mass again depends on the operating frequency of the vibration source. It is worth noting that heavier tip masses would create excessive strain on the beam, potentially inducing early fatigue failure. The weight of tip mass was selected as 40 g for the proposed MRPEH. This value was used for further analysis in the following sections and in the experiment. It was the largest tolerable weight by the branched beams before an obvious initial curvature occurs [46].

Table 4. First three resonant peaks for various masses obtained by ANSYS (NF: natural frequency).

M1 = M2 (g)	NF1 (Hz)	NF2 (Hz)	NF3 (Hz)
5	11.22	22.78	57.05
10	8.23	16.56	40.74
20	5.85	11.78	28.84
30	4.78	9.6	23.56
40	4.05	8.32	20.4
50	3.71	7.45	18.25
60	3.37	6.79	16.66
70	3.16	6.34	15.56
80	2.96	5.94	14.56
90	2.79	5.59	13.72
100	2.65	5.32	13.04

**Figure 2.** First three natural frequencies of the branched cantilever beam with varying masses obtained from ANSYS modal analysis (NF: natural frequency).

3.3. Modal and Harmonic Analysis of MRPEH

With the geometry of the branched beams and the weight of the tip masses determined, modal and harmonic analyses were further carried out in this section by considering the presence of the MFC patch, dimensioned $14 \times 28 \times 0.3$ mm, attached near the fixed end of the cantilever beam.

3.3.1. Modal Analysis

With the MFC patch attached to the cantilever beam, the results obtained from modal analysis were expected to differ slightly from those presented in Section 3.2. The first two resonance frequencies for the MRPEH are summarised in Table 5.

Table 5. Natural frequencies of the proposed MRPEH predicted by modal analysis using finite element analysis (FEA) (NF: natural frequency).

NF1 (a)	3.894
NF2 (b)	7.814
NF3 (c)	18.427
NF4 (d)	39.144
NF5 (e)	41.155
NF6 (f)	54.584

The total deformation shapes (of three main axes) for the first six resonance frequencies corresponding to Table 5 are illustrated in Figure 3. Note that the section in red represents the largest vertical displacement, which is an indication of the presence of resonances.

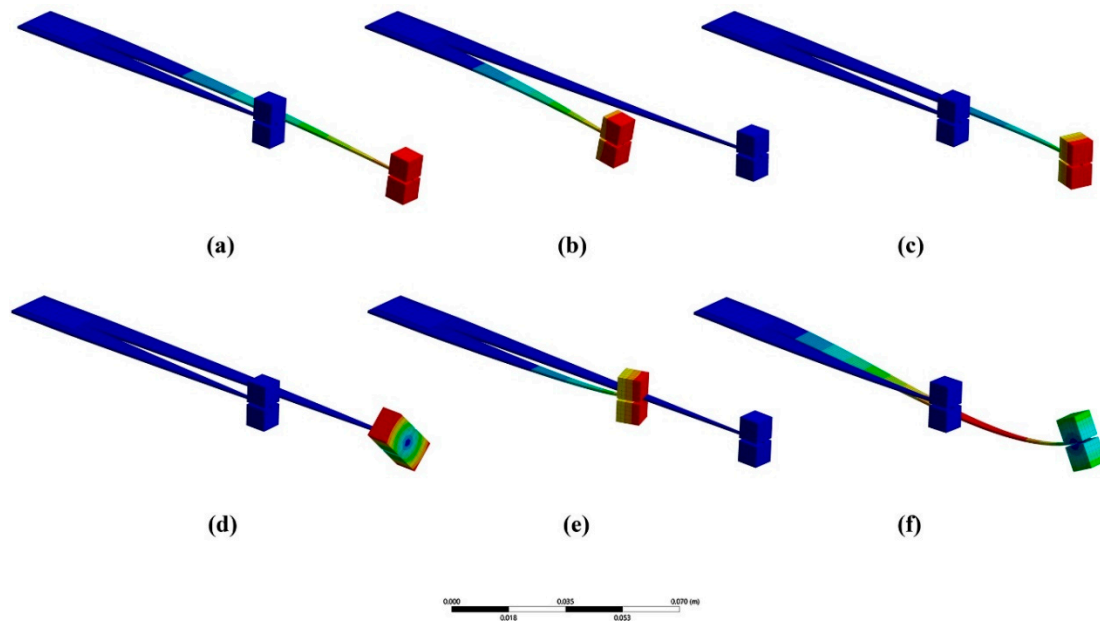


Figure 3. Deformation shapes of first six resonances of MRPEH obtained from ANSYS modal analysis. (a) NF1; (b) NF2; (c) NF3; (d) NF4; (e) NF5; (f) NF6 (NF: Natural Frequency).

In Figure 3a, the tip of the longer branch is in red, indicating that the longer branch is at its fundamental resonance (flexural mode). This corresponds to Case (a) in Table 5, with natural frequency of 3.89 Hz. On the other hand, Figure 3b shows the tip of the shorter branch in red, indicating that the shorter branch is at its fundamental resonance (flexural mode). This corresponds to Case (b) in Table 5, with a natural frequency of 7.81 Hz.

Note that the MFC patch would experience higher strain at resonances which results in power enhancement. Figure 3a,b justify that the proposed MRPEH has the capability to generate higher power across two close resonant frequencies below 10 Hz.

Figure 3c–f show the displacement of the MRPEH corresponding to the third to sixth resonances. These resonances include other modes such as the torsional mode of each branched beams. Since these modes are beyond the interest of this study, they are not further analysed.

3.3.2. Harmonic Analysis

Harmonic response analysis was also conducted to verify the outcome of the modal analysis. In this study, a base excitation of 0.2g was applied at the fixed end of the MRPEH. The frequency response, in terms of stress, strain and voltage from the MFC patch were calculated. The range of frequency considered was again between 1 Hz to 10 Hz. The outcome is graphically presented in Figures 4 and 5. For ease of comparison, the first two resonances obtained from modal analyses are also plotted in the figures. Observing Figure 4a,b, largest stress and strain are attained when the frequencies are closed to the resonance frequencies obtained from the modal analysis, which are the first two natural frequencies of the MRPEH (3.89 Hz and 7.81 Hz). This indicates that both harmonic response analysis and modal analysis agree closely with each other.

The voltage against frequency response, as illustrated in Figure 5, shows similar behaviour in which peak voltage is achieved at both resonance frequencies. The first resonance frequency yields a maximum voltage of 21.69 V and the second resonance produces 9.3 V. It is worth mentioning that there is a valley between the two resonance peaks. This valley is a result of an antiresonant phenomenon [59–62], which is unavoidable in multi-DOF systems [46].

In the next stage, a physical MRPEH prototype was fabricated and experimentally studied.

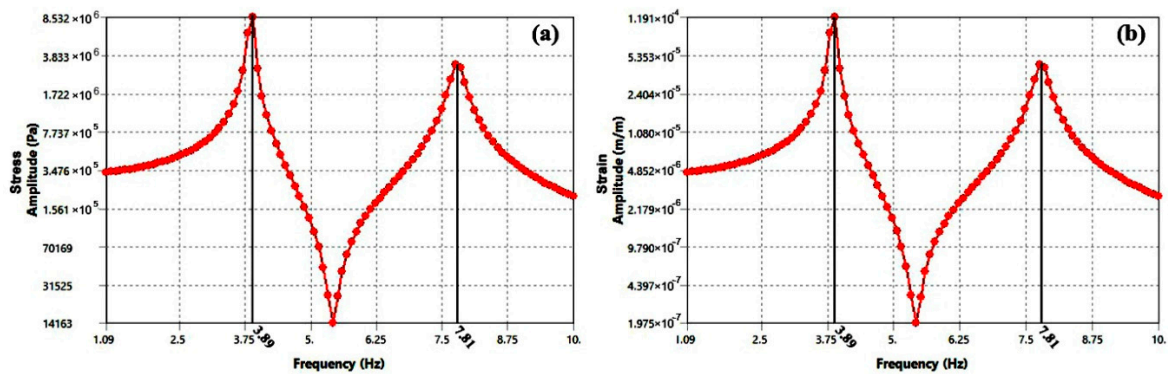


Figure 4. Frequency responses of MRPEH (a) stress and (b) strain obtained from FEA under 0.2g base excitation.

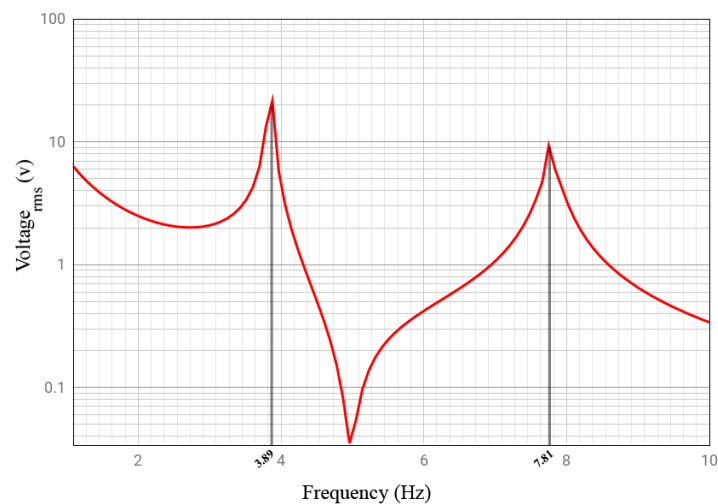


Figure 5. Voltage (log scale) against frequency response of MRPEH obtained from FEA under 0.2g base excitation.

4. Experimental Verification

4.1. Experimental Setup

An experimental study was carried out to analyse the performance of the proposed MRPEH and to verify the results obtained from the FEA. The MRPEH prototype was fabricated according to the design used for harmonic analysis (i.e., Design no. 2 of Table 3, with tip masses of 40 g each). The prototype consists of an aluminium (A 7075-T6) cantilever beam with two triangular branches and an MFC (M2814-P2, Smart Material GmbH, Dresden, Germany) patch. The MFC was bonded near the end of the main cantilever beam. MFC was chosen because of its flexibility and durability under repetitive bending motion, as compared to piezoceramics. The size of the MFC patch was carefully chosen to cover the width of the beam.

The MRPEH was excited by an electrodynamic shaker (APS-113, APS Dynamics, Inc.) at the fixed end. This long-stroke shaker has the ability to emulate low frequency vibrations. A vibration controller (SPEKTRA, Dresden, Germany) was used to drive the shaker through a power amplifier (APS125, APS Dynamics). The acceleration was measured at the fixed base of the cantilever beam through an accelerometer (Dytran 3305A2, 0.3 to 5000 Hz, $\pm 5\%$). The acceleration and the voltage generated were recorded by NI DAQ modules, NI 9234 and NI 9229, respectively, through Signal Express software. The schematic of the experimental setup and the fabricated prototype are shown in Figure 6a,b, respectively. Similar to the FEA, the MRPEH was excited under harmonic base excitation

in low frequency vibration range (1 Hz to 10 Hz). Accelerations of 0.05g, 0.1g and 0.2g were applied to the fixed end of the MRPEH.

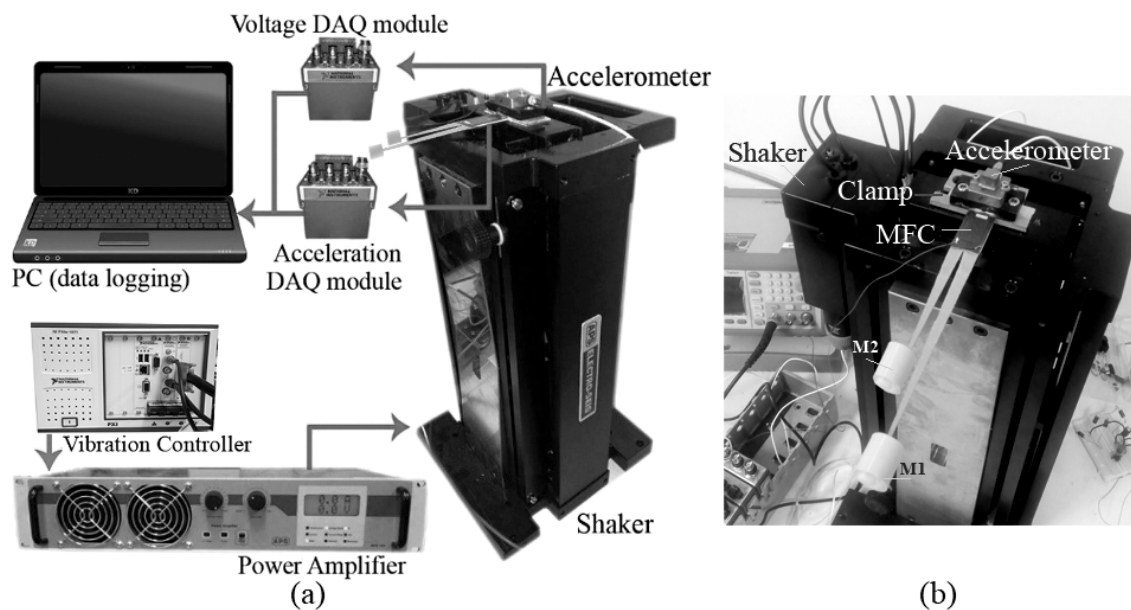


Figure 6. Schematic of (a) the experimental setup and (b) the fabricated MRPEH prototype attached on the shaker.

Two separate experimental tests were conducted. Firstly, the frequency range of interest was swept through and the open circuit voltage generated by the MRPEH was measured. The outcome was then compared to the numerical counterparts, as described in Section 4.2.1.

In the second experiment, the performance of the proposed MRPEH was further investigated by comparing its open circuit voltage to a similar PEHCB. This PEHCB consists of a rectangular aluminium beam ($0.21 \times 0.02 \times 0.001 \text{ m}^3$) with the surface-bonded piezoelectric patch (M2814-P2, Smart Materials Corp). An 80 g tip mass was attached at the end of the PEHCB. The results and discussions of the second test are presented in Section 4.2.2.

4.2. Results and Discussions

4.2.1. Comparison of Experiment and FEA

Figure 7a demonstrates the open voltages harvested from 1 to 10 Hz under three different base accelerations (0.05g, 0.1g, 0.2g). The MRPEH generated 18.44 V and 7.65 V at first (3.97 Hz) and second (7.66 Hz) resonant frequencies, respectively, under 0.2g base excitation. This amount dropped steadily when the base acceleration was decreased to 0.1g and 0.05g, as shown in Figure 7a.

Figure 7b illustrates the comparison between open circuit voltage recorded from the FEA and the experiment. The experimental results are found to match closely with the numerical outcome. This outcome further demonstrates that the proposed MRPEH is able to harvest high voltages at two close resonance frequencies below 10 Hz. The experimental results also verify the accuracy of the FE model.

The outcome from the study shows that the FE model is useful in optimising the geometry and tip mass of the proposed MRPEH. This effectively reduces the cost and labour required in experimental testing.

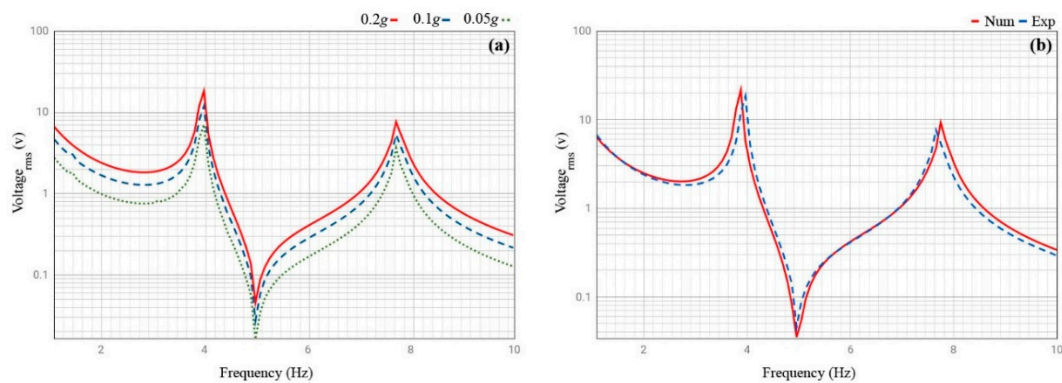


Figure 7. (a) Open voltages of MRPEH against frequency under various base excitations (b) Comparison of open circuit voltage output between experiment and numerical analysis at base excitation of 0.2g.

4.2.2. Comparison of MRPEH and Conventional PEHCB

In the second experiment, the output open circuit voltage of the proposed MRPEH was measured and compared to the conventional PEHCB under two scenarios. In the first scenario, the first two resonances of the MRPEH were selected as the frequencies of excitation. In the second scenario, several nonresonance frequencies below 10 Hz were excited. Acceleration of 0.2g was again applied as base excitation for both scenarios. Both harvesters were placed on the shaker with their voltages simultaneously measured.

(1) Responses at Resonance

Figure 8a,b illustrates the open circuit voltage harvested by the MRPEH and the conventional PEHCB at the first two resonance frequencies of the MRPEH, i.e., at approximately 3.97 Hz and 7.66 Hz, respectively. It can be clearly seen that the MRPEH produced much higher voltages at both frequencies as compared to the PEHCB.

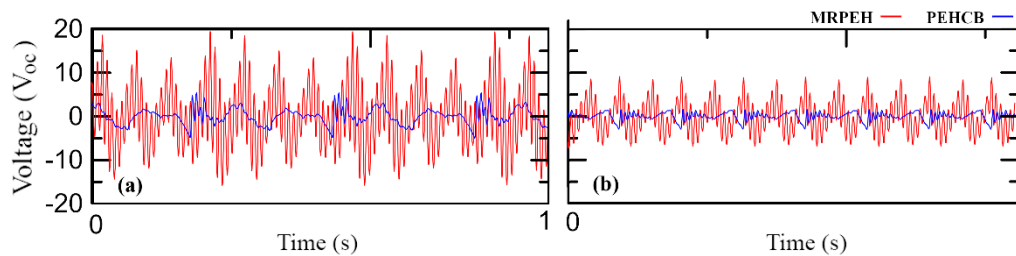


Figure 8. Comparison of open circuit voltage harvested from MRPEH and conventional PEHCB at (a) 3.97 Hz and (b) 7.66 Hz.

(2) Responses at Nonresonance

It was found that no resonance exists for the conventional PEHCB below 10 Hz. For the sake of comparison, several discrete frequencies outside of the two resonances of the MRPEH were selected. Figure 9 illustrates the open circuit voltage harvested from both harvesters at these frequencies.

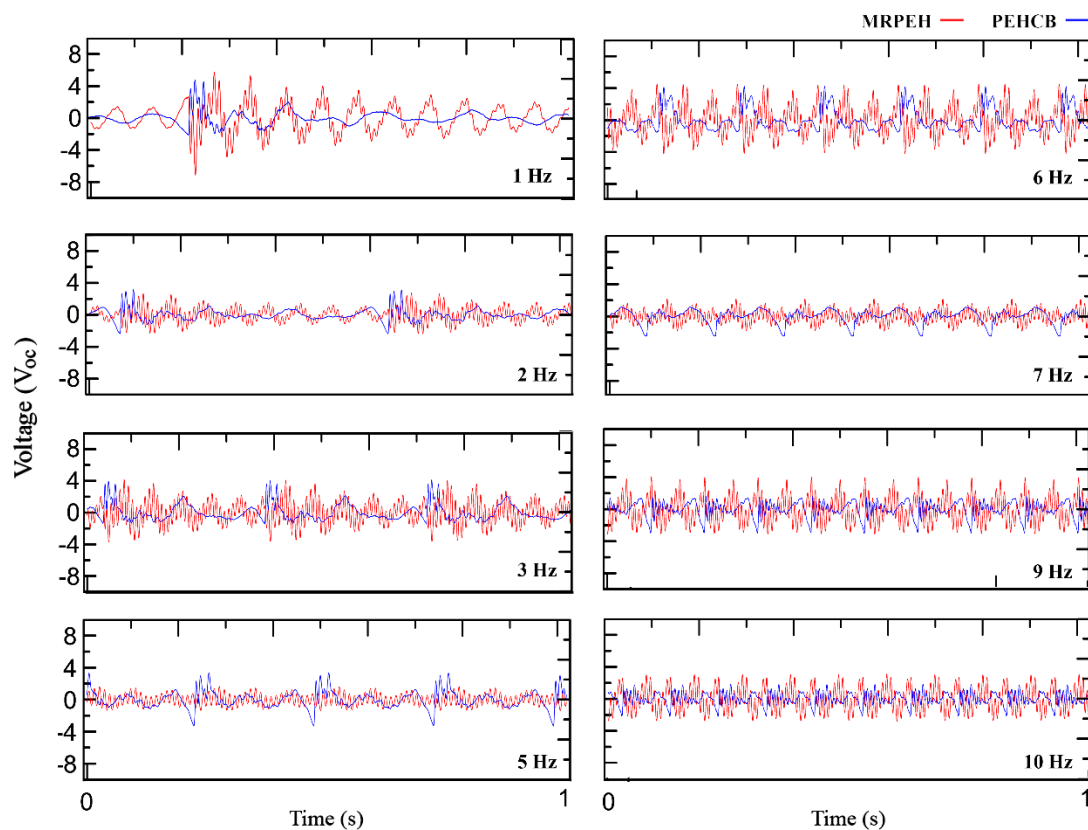


Figure 9. Comparison of open circuit voltage harvested from MRPEH and conventional PEHCB at nonresonance frequencies below 10 Hz.

The MRPEH was generally able to generate a higher or similar voltage at these nonresonance frequencies, in comparison to the PEHCB. An exception was noted at 5 Hz where the MRPEH was outperformed by the PEHCB due to the antiresonance phenomenon of the MRPEH.

Observing Figure 9, another advantage of the MRPEH in comparison to the PEHCB can be identified; after each impact, the voltage generated from PEHCB damped quickly with time. However, the voltage generated by MRPEH remained at a higher level for a longer period of time. In other words, the idle time between two impacts is much shorter for the MRPEH in comparison to the PEHCB. This effect is particularly pronounced when the frequency is low (less than 3 Hz). Thus, it can be concluded that the overall efficiency of the MRPEH is higher than the PEHCB, regardless of the frequency of excitation.

5. Conclusions

This study attempted to improve the performance of MRPEH with the use of a cantilever beam with two triangular branches and through optimisation of various design parameters. The proposed MRPEH is capable of harvesting energy from broadband, low frequency (1–10 Hz) and low amplitude ambient vibration sources. Design optimisation is achieved by performing a parametric study using FEM on the geometries of the branched beams and the weight of the tip masses to search for two close resonance frequencies. The proposed MRPEH was found to be able to produce two close resonance frequencies under 0.2g excitation below 10 Hz. The model was also experimentally verified. Results show that the proposed MRPEH has the potential to perform broadband energy harvesting from ambient vibration sources and is superior to a similar PEHCB, which is commonly used in various applications.

For future work, it is recommended that more than two branched beams can be attempted. The use of a circular base can also potentially improve the design. Study related to reducing the negative impact of the antiresonance is also highly recommended.

Author Contributions: Conceptualization, I.I. and Y.Y.L.; methodology, I.I., Y.Y.L. and R.V.P.; software, I.I. and M.S.; validation, I.I., R.V.P. and Y.Y.L.; formal analysis, I.I.; investigation, J.P.N.; resources, J.P.N.; data curation, I.I.; writing—original draft preparation, I.I.; writing—review and editing, I.I., R.V.P., M.S., J.P.N. and Y.Y.L.; visualization, I.I.; supervision, Y.Y.L. and R.V.P.; project administration, I.I.; funding acquisition, R.V.P.

Funding: This research received no external funding.

Conflicts of Interest: The authors declare no conflict of interest.

References

1. Chabane, F.; Moummi, N.; Benramache, S. *Experimental Study on Heat Transfer of Solar Air Heater*; LAP Lambert Academic Publishing: Saarbrücken, Germany, 2013.
2. Chabane, F.; Moummi, N.; Benramache, S. Experimental study of heat transfer and thermal performance with longitudinal fins of solar air heater. *J. Adv. Res.* **2014**, *5*, 183–192. [[CrossRef](#)] [[PubMed](#)]
3. Chabane, F.; Moummi, N.; Benramache, S.; Bensahal, D.; Belahssen, O.; Lemmadi, F. Thermal performance optimization of a flat plate solar air heater. *Int. J. Energy Technol.* **2013**, *5*, 1–6.
4. Hajmohammadi, M.; Aghajannezhad, P.; Abolhassani, S.; Parsaee, M. An integrated system of zinc oxide solar panels, fuel cells, and hydrogen storage for heating and cooling applications. *Int. J. Hydrog. Energy* **2017**, *42*, 19683–19694. [[CrossRef](#)]
5. Hajmohammadi, M. Introducing a ψ -shaped cavity for cooling a heat generating medium. *Int. J. Therm. Sci.* **2017**, *121*, 204–212. [[CrossRef](#)]
6. Sedighi, M.; Padilla, R.V.; Taylor, R.A.; Lake, M.; Izadgoshasb, I.; Rose, A. High-temperature, point-focus, pressurised gas-phase solar receivers: A comprehensive review. *Energy Convers. Manag.* **2019**, *185*, 678–717. [[CrossRef](#)]
7. Zappalá, D.; Sarma, N.; Djurović, S.; Crabtree, C.; Mohammad, A.; Tavner, P. Electrical & mechanical diagnostic indicators of wind turbine induction generator rotor faults. *Renew. Energy* **2019**, *131*, 14–24.
8. Wang, Y.; Xu, Y.; Lei, Y. An effect assessment and prediction method of ultrasonic de-icing for composite wind turbine blades. *Renew. Energy* **2018**, *118*, 1015–1023. [[CrossRef](#)]
9. Antonini, E.G.; Romero, D.A.; Amon, C.H. Improving CFD wind farm simulations incorporating wind direction uncertainty. *Renew. Energy* **2019**, *133*, 1011–1023. [[CrossRef](#)]
10. Kan, J.; Fan, C.; Wang, S.; Zhang, Z.; Wen, J.; Huang, L. Study on a piezo-windmill for energy harvesting. *Renew. Energy* **2016**, *97*, 210–217. [[CrossRef](#)]
11. Brand, O.; Fedder, G.K.; Hierold, C.; Korvink, J.G.; Tabata, O. *Micro Energy Harvesting*; John Wiley & Sons: Hoboken, NJ, USA, 2015.
12. Bunn, D.W.; Redondo-Martin, J.; Muñoz-Hernandez, J.I.; Diaz-Cachinero, P. Analysis of coal conversion to biomass as a transitional technology. *Renew. Energy* **2019**, *132*, 752–760. [[CrossRef](#)]
13. San Juan, J.L.G.; Aviso, K.B.; Tan, R.R.; Sy, C.L. A Multi-Objective Optimization Model for the Design of Biomass Co-Firing Networks Integrating Feedstock Quality Considerations. *Energies* **2019**, *12*, 2252. [[CrossRef](#)]
14. Liu, H.; Maghoul, P.; Bahari, A.; Kavgic, M. Feasibility study of snow melting system for bridge decks using geothermal energy piles integrated with heat pump in Canada. *Renew. Energy* **2019**, *136*, 1266–1280. [[CrossRef](#)]
15. Turkmen, A.C.; Celik, C. Energy harvesting with the piezoelectric material integrated shoe. *Energy* **2018**, *150*, 556–564. [[CrossRef](#)]
16. Elahi, H.; Eugeni, M.; Gaudenzi, P. A review on mechanisms for piezoelectric-based energy harvesters. *Energies* **2018**, *11*, 1850. [[CrossRef](#)]
17. Lim, Y.Y.; Smith, S.T.; Izadgoshasb, I. Smart-based monitoring of epoxy using piezoelectric transducers. In Proceedings of the SHMII 2017—8th International Conference on Structural Health Monitoring of Intelligent Infrastructure, Brisbane, Australia, 5–8 December 2017; pp. 1151–1159.

18. Lim, Y.Y.; Izadgoshasb, I.; Smith, S.T. Monitoring of corrosion process in structural adhesive using smart materials. In Proceedings of the SHMII 2017—8th International Conference on Structural Health Monitoring of Intelligent Infrastructure, Brisbane, Australia, 5–8 December 2017; pp. 1186–1194.
19. Izadgoshasb, I.; Lim, Y.Y.; Tang, L.; Padilla, R.V.; Tang, Z.S.; Sedighi, M. Improving efficiency of piezoelectric based energy harvesting from human motions using double pendulum system. *Energy Convers. Manag.* **2019**, *184*, 559–570. [[CrossRef](#)]
20. Tang, Z.S.; Lim, Y.Y.; Smith, S.T.; Izadgoshasb, I. Development of analytical and numerical models for predicting the mechanical properties of structural adhesives under curing using the PZT-based wave propagation technique. *Mech. Syst. Signal Process.* **2019**, *128*, 172–190. [[CrossRef](#)]
21. Lim, Y.Y.; Smith, S.T.; Soh, C.K. Wave propagation based monitoring of concrete curing using piezoelectric materials: Review and path forward. *NDT E Int.* **2018**, *99*, 50–63. [[CrossRef](#)]
22. Syta, A.; Litak, G.; Friswell, M.I.; Adhikari, S. Multiple solutions and corresponding power output of a nonlinear bistable piezoelectric energy harvester. *Eur. Phys. J. B* **2016**, *89*, 99. [[CrossRef](#)]
23. Wolszczak, P.; Łygas, K.; Litak, G. Dynamics identification of a piezoelectric vibrational energy harvester by image analysis with a high speed camera. *Mech. Syst. Signal Process.* **2018**, *107*, 43–52. [[CrossRef](#)]
24. Hosseini, R.; Hamed, M. Resonant frequency of bimorph triangular V-shaped piezoelectric cantilever energy harvester. *J. Comput. Appl. Res. Mech. Eng.* **2016**, *6*, 65–73.
25. Benasciutti, D.; Moro, L.; Zelenika, S.; Brusa, E. Vibration energy scavenging via piezoelectric bimorphs of optimized shapes. *Microsyst. Technol.* **2010**, *16*, 657–668. [[CrossRef](#)]
26. Li, W.G.; He, S.; Yu, S. Improving power density of a cantilever piezoelectric power harvester through a curved L-shaped proof mass. *IEEE Trans. Ind. Electron.* **2010**, *57*, 868–876. [[CrossRef](#)]
27. Ou, Q.; Chen, X.; Gutschmidt, S.; Wood, A.; Leigh, N.; Arrieta, A.F. An experimentally validated double-mass piezoelectric cantilever model for broadband vibration-based energy harvesting. *J. Intell. Mater. Syst. Struct.* **2012**, *23*, 117–126. [[CrossRef](#)]
28. Kashiwao, T.; Izadgoshasb, I.; Lim, Y.Y.; Deguchi, M. Optimization of rectifier circuits for a vibration energy harvesting system using a macro-fiber composite piezoelectric element. *Microelectron. J.* **2016**, *54*, 109–115. [[CrossRef](#)]
29. Wickenheiser, A.M.; Garcia, E. Power optimization of vibration energy harvesters utilizing passive and active circuits. *J. Intell. Mater. Syst. Struct.* **2010**, *21*, 1343–1361. [[CrossRef](#)]
30. Anton, S.R.; Sodano, H.A. A review of power harvesting using piezoelectric materials (2003–2006). *Smart Mater. Struct.* **2007**, *16*, R1. [[CrossRef](#)]
31. Narita, F.; Fox, M. A review on piezoelectric, magnetostrictive, and magnetoelectric materials and device technologies for energy harvesting applications. *Adv. Eng. Mater.* **2018**, *20*, 1700743. [[CrossRef](#)]
32. Ramalingam, U.; Gandhi, U.; Mangalanathan, U.; Choi, S.-B. A new piezoelectric energy harvester using two beams with tapered cavity for high power and wide broadband. *Int. J. Mech. Sci.* **2018**, *142*, 224–234. [[CrossRef](#)]
33. Challa, V.R.; Prasad, M.; Shi, Y.; Fisher, F.T. A vibration energy harvesting device with bidirectional resonance frequency tunability. *Smart Mater. Struct.* **2008**, *17*, 015035. [[CrossRef](#)]
34. Hu, Y.; Xue, H.; Hu, H. A piezoelectric power harvester with adjustable frequency through axial preloads. *Smart Mater. Struct.* **2007**, *16*, 1961. [[CrossRef](#)]
35. Ferrari, M.; Ferrari, V.; Guizzetti, M.; Marioli, D.; Taroni, A. Piezoelectric multifrequency energy converter for power harvesting in autonomous microsystems. *Sens. Actuators A Phys.* **2008**, *142*, 329–335. [[CrossRef](#)]
36. Erturk, A.; Renno, J.M.; Inman, D.J. Modeling of piezoelectric energy harvesting from an L-shaped beam-mass structure with an application to UAVs. *J. Intell. Mater. Syst. Struct.* **2008**, *20*, 529–544. [[CrossRef](#)]
37. Kim, I.-H.; Jung, H.-J.; Lee, B.M.; Jang, S.-J. Broadband energy-harvesting using a two degree-of-freedom vibrating body. *Appl. Phys. Lett.* **2011**, *98*, 214102. [[CrossRef](#)]
38. Wu, H.; Tang, L.; Yang, Y.; Soh, C.K. A novel two-degrees-of-freedom piezoelectric energy harvester. *J. Intell. Mater. Syst. Struct.* **2013**, *24*, 357–368. [[CrossRef](#)]
39. Zhang, G.; Hu, J. A branched beam-based vibration energy harvester. *J. Electron. Mater.* **2014**, *43*, 3912–3921. [[CrossRef](#)]
40. Stanton, S.C.; McGehee, C.C.; Mann, B.P. Reversible hysteresis for broadband magnetopiezoelectric energy harvesting. *Appl. Phys. Lett.* **2009**, *95*, 174103. [[CrossRef](#)]

41. Wu, W.-J.; Chen, Y.-Y.; Lee, B.-S.; He, J.-J.; Peng, Y.-T. Tunable resonant frequency power harvesting devices. In Proceedings of the Smart Structures and Materials 2006: Damping and Isolation, San Diego, CA, USA, 26 February–2 March 2006; p. 61690A.
42. Tang, L.; Yang, Y. A nonlinear piezoelectric energy harvester with magnetic oscillator. *Appl. Phys. Lett.* **2012**, *101*, 094102. [[CrossRef](#)]
43. Tang, L.; Yang, Y.; Soh, C.K. Toward broadband vibration-based energy harvesting. *J. Intell. Mater. Syst. Struct.* **2010**, *21*, 1867–1897. [[CrossRef](#)]
44. Sordo, G.; Serra, E.; Schmid, U.; Iannacci, J. Optimization method for designing multimodal piezoelectric MEMS energy harvesters. *Microsyst. Technol.* **2016**, *22*, 1811–1820. [[CrossRef](#)]
45. Wu, M.; Ou, Y.; Mao, H.; Li, Z.; Liu, R.; Ming, A.; Ou, W. Multi-resonant wideband energy harvester based on a folded asymmetric M-shaped cantilever. *Aip Adv.* **2015**, *5*, 077149. [[CrossRef](#)]
46. Upadrashta, D.; Yang, Y. Trident-Shaped Multimodal Piezoelectric Energy Harvester. *J. Aerosp. Eng.* **2018**, *31*, 04018070. [[CrossRef](#)]
47. Li, X.; Upadrashta, D.; Yu, K.; Yang, Y. Analytical modeling and validation of multi-mode piezoelectric energy harvester. *Mech. Syst. Signal Process.* **2019**, *124*, 613–631. [[CrossRef](#)]
48. Basari, A.A.; Awaji, S.; Wang, S.; Hashimoto, S.; Kumagai, S.; Suto, K.; Okada, H.; Okuno, H.; Himm, B.; Jiang, W. Shape effect of piezoelectric energy harvester on vibration power generation. *J. Power Energy Eng.* **2014**, *2*, 117–124. [[CrossRef](#)]
49. Izadgoshasb, I.; Lim, Y.Y.; Lake, N.; Tang, L.; Padilla, R.V.; Kashiwao, T. Optimizing orientation of piezoelectric cantilever beam for harvesting energy from human walking. *Energy Convers. Manag.* **2018**, *161*, 66–73. [[CrossRef](#)]
50. Dietl, J.M.; Garcia, E. Beam shape optimization for power harvesting. *J. Intell. Mater. Syst. Struct.* **2010**, *21*, 633–646. [[CrossRef](#)]
51. Friswell, M.; Mottershead, J.E. *Finite Element Model Updating in Structural Dynamics*; Springer Science & Business Media: Dordrecht, The Netherlands, 2013; Volume 38.
52. Elvin, N.G.; Elvin, A.A. A coupled finite element—Circuit simulation model for analyzing piezoelectric energy generators. *J. Intell. Mater. Syst. Struct.* **2009**, *20*, 587–595. [[CrossRef](#)]
53. Yang, Y.; Tang, L. Equivalent circuit modeling of piezoelectric energy harvesters. *J. Intell. Mater. Syst. Struct.* **2009**, *20*, 2223–2235. [[CrossRef](#)]
54. Arafa, M.; Akl, W.; Aladwani, A.; Aldraihem, O.; Baz, A. Experimental implementation of a cantilevered piezoelectric energy harvester with a dynamic magnifier. In Proceedings of the 2011 Active and Passive Smart Structures and Integrated Systems, San Diego, CA, USA, 7–10 March 2011; p. 79770Q.
55. Thein, C.K.; Liu, J.-S. Numerical modeling of shape and topology optimisation of a piezoelectric cantilever beam in an energy-harvesting sensor. *Eng. Comput.* **2017**, *33*, 137–148. [[CrossRef](#)]
56. Dutoit, N.E.; Wardle, B.L.; Kim, S.-G. Design considerations for MEMS-scale piezoelectric mechanical vibration energy harvesters. *Integr. Ferroelectr.* **2005**, *71*, 121–160. [[CrossRef](#)]
57. Goldfarb, M.; Celanovic, N. A lumped parameter electromechanical model for describing the nonlinear behavior of piezoelectric actuators. *J. Dyn. Syst. Meas. Control* **1997**, *119*, 478–485. [[CrossRef](#)]
58. Gallas, Q.; Holman, R.; Nishida, T.; Carroll, B.; Sheplak, M.; Cattafesta, L. Lumped element modeling of piezoelectric-driven synthetic jet actuators. *AIAA J.* **2003**, *41*, 240–247. [[CrossRef](#)]
59. Van de Vorst, E.; Van Campen, D.; De Kraker, A.; Fey, R. Periodic solutions of a multi-DOF beam system with impact. *J. Sound Vib.* **1996**, *192*, 913–925. [[CrossRef](#)]
60. Welte, J.; Kniffka, T.J.; Ecker, H. Parametric excitation in a two degree of freedom MEMS system. *Shock Vib.* **2013**, *20*, 1113–1124. [[CrossRef](#)]
61. Comparin, R.J.; Singh, R. Frequency response characteristics of a multi-degree-of-freedom system with clearances. *J. Sound Vib.* **1990**, *142*, 101–124. [[CrossRef](#)]
62. Rustighi, E.; Brennan, M.; Mace, B. A shape memory alloy adaptive tuned vibration absorber: Design and implementation. *Smart Mater. Struct.* **2004**, *14*, 19. [[CrossRef](#)]

